Adv. Comp. Letts., in press (2005)

Generalized Shear-Lag Analysis Including Imperfect Interfaces

J. A. NAIRN
Material Science and Engineering, University of Utah, Salt Lake City, Utah 84112, USA

Abstract

Two recent papers showed that shear-lag analysis can be an effective tool for stress analysis of composites when done properly and when applied to problems for which it is appropriate. This paper extends the prior analysis of concentric cylinders to a generalized shear-lag analysis in which the transverse variations of shear stress are described by arbitrary shape functions. The shear-lag analysis and solution can be derived in terms of averages of the new shape functions. The shape functions can be specified after analysis and tailored to suit specific problems. This paper also extends shear-lag analysis of both concentric cylinders and multilayered structures to model imperfect interfaces between the layers. The generalized methods were applied to several issues in fiber/matrix stress transfer modeled as two concentric cylinders. By modifying prior shape functions, it was possible to extend shear-lag analysis to work for any fiber volume fraction. Prior shear-lag models were all unacceptable at low fiber volume fraction. The full shear-lag analysis can model stress transfer for both isotropic and anisotropic fibers. The new imperfect interface capability was used to interpret experimental results for fiber/matrix stress transfer in terms of interface quality.

Introduction

Two prior papers presented new shear-lag methods for stress-transfer calculations in concentric cylinders[1] or in multilayered structures.[2] Both analyses started with the fundamental shear-lag assumption that expresses in-plane shear stresses as

$$\tau_{rz} \propto \frac{\partial w}{\partial r} \qquad \text{or} \qquad \tau_{xy} \propto \frac{\partial v}{\partial x} \tag{1}$$

In other words, the shear strain was simplified by assuming

$$\left|\frac{\partial u}{\partial z}\right| << \left|\frac{\partial w}{\partial r}\right| \qquad \text{or} \qquad \left|\frac{\partial u}{\partial y}\right| << \left|\frac{\partial v}{\partial x}\right| \tag{2}$$

Here u and w are the r and z direction displacements in cylinder analysis and u and v are the x and y direction displacements in planar analysis (see Figs. 1 and 2). Unfortunately, the fundamental shear-lag assumptions were not sufficient for derivation of shear-lag equations.[1,2] To derive shear-lag equations, the next key assumptions were to postulate a form for the shear stresses in each cylinder or layer. Following McCartney,[3] the cylindrical, shear-lag analysis assumed the shear stress in concentric cylinder i has the form

$$\tau_{rz}^{(i)}(r,z) = \frac{f_0^{(i)}(z)r}{2} + \frac{f_1^{(i)}(z)}{r} \tag{3}$$

where $f_0^{(i)}(z)$ and $f_1^{(i)}(z)$ are two arbitrary functions of z for cylinder i (see Fig. 1). Combining the fundamental shear-lag and shear-stress assumptions with two simplifications in the constitutive law, it was possible to derive a system of equations for finding all axial and shear stresses in a collection of concentric cylinders. This analysis was termed the "optimal" shear-lag analysis for cylindrical coordinates.[1] For the fiber/matrix problem (two cylinders — a fiber surrounded by a matrix), the optimal shear-lag analysis is identical to prior solutions by McCartney[3] and Nayfeh.[4] Optimal shear-lag analysis agrees well with finite element calculations provided the interface is perfect and the fiber volume fraction is not too low.[1] Notably,

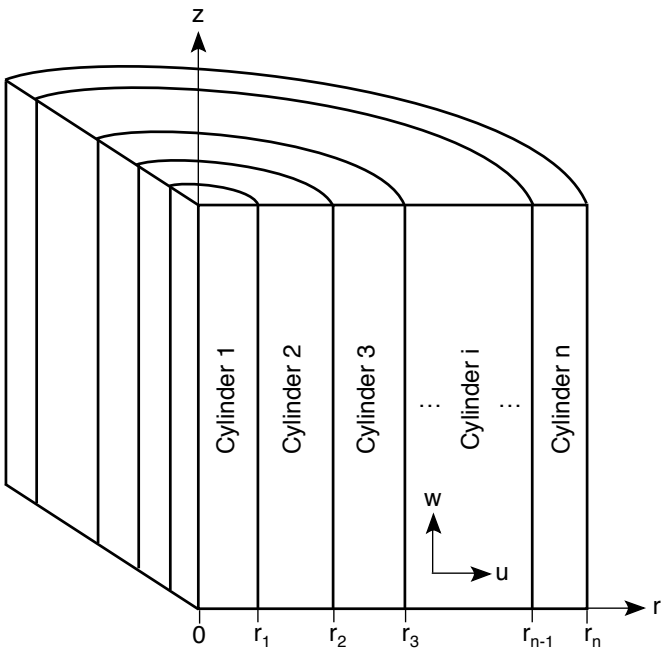

Fig. 1. A section of n concentric cylinders showing the r-z coordinate system for analysis. The displacements u and w are in the r and z directions, respectively. The central cylinder (cylinder 1) may be solid ($r_0 = 0$) as pictured or may be hollow ($r_0 > 0$).

the optimal shear-lag parameter is significantly different then the Cox[5] shear-lag parameter commonly used in the composites literature. Therefore, the Cox parameter should be replaced by the optimal shear-lag parameter.

The same analysis methods were subsequently applied to planar analysis of multilayered structures.[2] Instead of an explicit assumption about shear stresses, however, it was noted that the shear stresses could be expressed in terms of shape functions. The shear stress in layer i was written as

$$\tau_{xy}^{(i)}(x,y) = \tau(x_{i-1},y)L_i(z_i) + \tau(x_i,y)R_i(z_i) \qquad \text{where} \qquad z_i = \frac{x - x_{i-1}}{t_i} \tag{4}$$

where $\tau(x_i, y)$ is the interfacial shear stress for the interface located at x_i, $L_i(z_i)$ and $R_i(z_i)$ are the left and right shape functions of the dimensionless z_i coordinate, and layer i of thickness t_i extends from x_{i-1} to x_i (see Fig. 2). For continuity in interfacial shear stresses:

$$L_i(0) = 1, \qquad L_i(1) = 0, \qquad R_i(0) = 0, \qquad \text{and} \qquad R_i(1) = 1 \tag{5}$$

The advantage of using shape functions was that they could be left arbitrary throughout the shear-lag analysis. Shape function only need to be specified for final calculations. A shear-lag analysis with shape functions can be termed a "generalized" shear-lag analysis. An "optimal" shear-lag analysis is a special case of "generalized" shear-lag analysis with specific shape functions. For example, McCartney[3] derived an optimal shear-lag analysis for cross-ply laminates (symmetric, planar problem with two layers). The McCartney analysis is a special case of "generalized' shear-lag analysis using linear shape functions: $L_i(z_i) = 1 - z_i$ and $R_i(z_i) = z_i$. The availability of shape functions allows one to deviate from linear assumptions and improve accuracy for certain problems. For example, Nairn and Mendels[2,6] used non-linear shape functions to analyze a compression-loaded double-lap shear specimen. The choice of non-linear shape functions was guided by finite element calculations, which also confirmed excellent results for the final generalized shear-lag results.

The purpose of this paper is three fold. First, this paper extends the optimal shear-lag analysis for concentric cylinders in Ref. [1] to a generalized shear-lag analysis by expressing the shear stress in cylinder i as

$$r\tau_{rz}^{(i)}(r,z) = r_{i-1}\tau(r_{i-1},z)I_i(r) + r_i\tau(r_i,z)O_i(r) \tag{6}$$

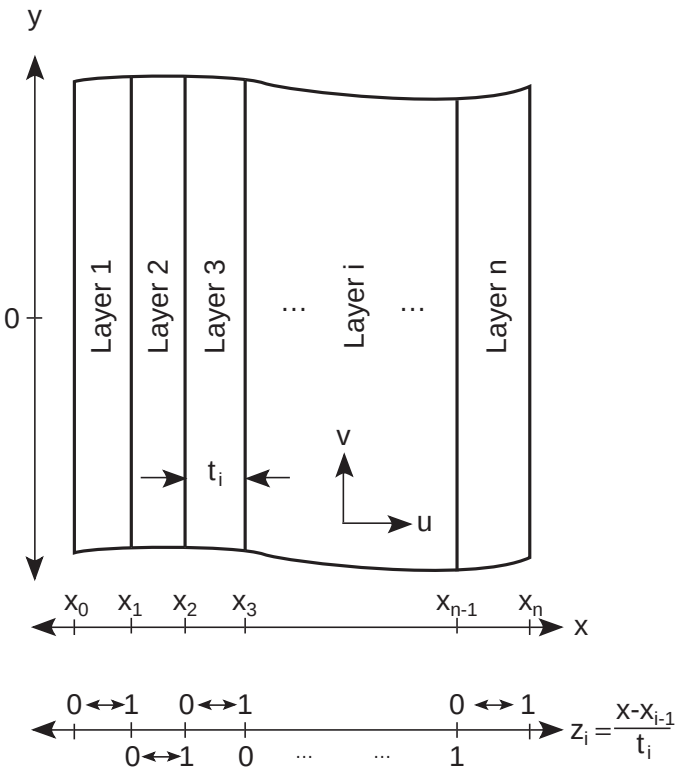

Fig. 2. A section of n layers showing the x-y coordinate system for analysis and the dimensionless z_i coordinate in each layer. The displacements u and v are in the x and y directions, respectively.

where $\tau(r_i, z)$ is the interfacial shear stress for the interface located at r_i, $I_i(r)$ and $O_i(r)$ are inner and outer shape functions, and cylinder i extends from r_{i-1} to r_i. For continuity in interfacial shear stresses:

$$I_i(r_{i-1}) = 1, \qquad I_i(r_i) = 0, \qquad O_i(r_{i-1}) = 0, \qquad \text{and} \qquad O_i(r_i) = 1 \tag{7}$$

This new generalized shear-lag analysis contains the prior optimal shear-lag analysis[1] as a special case. The optimal shear-lag analysis is recovered by setting

$$I_i(r) = \frac{r_i^2 - r^2}{r_i^2 - r_{i-1}^2} \qquad \text{and} \qquad O_i(r) = \frac{r^2 - r_{i-1}^2}{r_i^2 - r_{i-1}^2} \tag{8}$$

which are equivalent to Eq. (3) with

$$f_0^{(i)} = \frac{2}{r_i^2 - r_{i-1}^2}\big(r_i\tau(r_i, z) - r_{i-1}\tau(r_{i-1}, z)\big) \quad \text{and} \quad f_1^{(i)} = \frac{r_i r_{i-1}}{r_i^2 - r_{i-1}^2}\big(r_i\tau(r_{i-1}, z) - r_{i-1}\tau(r_i, z)\big) \tag{9}$$

The second purpose is to extend shear-lag analysis to handle imperfect interfaces. A feature of some prior shear-lag analyses is that their derivation exactly satisfies axial displacement (w or v) continuity at all interfaces.[1,2] If instead of enforcing interface continuity, one allows a discontinuity based on the current interfacial stress state, it is possible to implement imperfect interface modeling[7–10] into shear-lag analysis. Here, an imperfect interface was implemented by assuming axial displacement discontinuities given by

$$[w(r_i)] = w_{i+1}(r_i, z) - w_i(r_i, z) = \frac{\tau(r_i, z)}{D_s^{(i)}} \qquad \text{(concentric cylinders)} \tag{10}$$

$$[v(x_i)] = v_{i+1}(x_i, z) - v_i(x_i, z) = \frac{\tau(x_i, z)}{D_s^{(i)}} \qquad \text{(multilayers)} \tag{11}$$

where $[w(r_i)]$ and $[v(x_i)]$ are axial displacement discontinuities for the interfaces at r_i or x_i, $w_i(r_i,z)$ and $v_i(x_i,z)$ are axial displacements in cylinder or layer i, and $D_s^{(i)}$ is an imperfect interface parameter for the interface between cylinder or layer i and cylinder or layer $i+1$. $D_s^{(i)}=\infty$ results in zero discontinuity or a perfect interface. $D_s^{(i)}=0$ results in zero interfacial shear stress or a debonded interface. Values between zero and infinity model an imperfect interface.[7] Imperfect interfaces may additionally have radial or transverse displacement discontinuities that are proportional to the interfacial normal stress.[7] The shear-lag analysis derived here can only model axial displacement discontinuities.

The third purpose is to use the new generalized analysis for concentric cylinders to consider two prior problems with shear-lag analysis. First, all prior shear-lag analyses for stress transfer in fiber/matrix problems break down for low fiber volume fraction. The problem is that shear-lag parameters, such as the optimal Nayfeh[1,3,4] or Cox[5] parameter, approach zero as fiber volume fraction approaches zero. A common practice to avoid this problem is to introduce an *effective* fiber volume fracture or, equivalently, to assume an *effective* radius of the outer cylinder enclosing the fiber cylinder. The problem with analyses based on *effective* properties is that they introduce unknown parameters. By modifying shape functions, it is possible to derive a shear-lag analysis that works for all fiber volume fractions and eliminates the need for resorting to effective volume fraction or outer-cylinder radius. Second, many prior shear-lag analyses have used the Cox parameter. Using generalized shear-lag analysis, it is possible to show that the Cox parameter is a special case that corresponds to certain shape functions. Examination of "Cox" shape functions illustrates the fundamental problems with the Cox parameter.

Generalized Shear-Lag Analysis

The derivation of a generalized shear-lag analysis for cylindrical problems follows the derivation of the optimal shear-lag analysis in Ref. [1] except that the shear stresses are expressed using shape functions (see Eq. (6)). The first step is a transform technique used by McCartney[3] — equate $\tau_{rz}^{(i)}(r,z)$ in terms of shape functions to the fundamental shear-lag assumption

$$\tau_{rz}^{(i)}(r,z)=G_A^{(i)}\frac{\partial w}{\partial r}, \tag{12}$$

multiply both sides by $(A-r^2)$, where A is a constant, and integrate by parts from r_{i-1} to r_i. Here $G_A^{(i)}=G_{rz}^{(i)}$ is the axial shear modulus of cylinder i. The derivation, which also includes a simplification of the axial Hooke's law, proceeds exactly as in Ref. [1] resulting in new generalized results for axial displacement derivatives with respect to z on the two interfaces of the cylinder:

$$\begin{aligned} w_i''(r_i,z) &= \frac{2}{E_A^{(i)}(r_i^2-r_{i-1}^2)}\left[r_{i-1}\tau(r_{i-1},z)-r_i\tau(r_i,z)\right]-\frac{1}{2G_A^{(i)}}\left[r_{i-1}\tau''(r_{i-1},z)\left\langle\left(\frac{r_{i-1}^2}{r^2}-1\right)I_i(r)\right\rangle\right. \\ &\qquad \left. +\, r_i\tau''(r_i,z)\left\langle\left(\frac{r_{i-1}^2}{r^2}-1\right)O_i(r)\right\rangle\right] \end{aligned} \tag{13}$$

$$\begin{aligned} w_i''(r_{i-1},z) &= \frac{2}{E_A^{(i)}(r_i^2-r_{i-1}^2)}\left[r_{i-1}\tau(r_{i-1},z)-r_i\tau(r_i,z)\right]-\frac{1}{2G_A^{(i)}}\left[r_{i-1}\tau''(r_{i-1},z)\left\langle\left(\frac{r_i^2}{r^2}-1\right)I_i(r)\right\rangle\right. \\ &\qquad \left. +\, r_i\tau''(r_i,z)\left\langle\left(\frac{r_i^2}{r^2}-1\right)O_i(r)\right\rangle\right] \end{aligned} \tag{14}$$

where $E_A^{(i)}=E_{zz}^{(i)}$ is the axial modulus of cylinder i and angle brackets indicate averaging over the cross-section of a cylindrical shell:

$$\langle f(r)\rangle=\frac{1}{\pi(r_i^2-r_{i-1}^2)}\int_{r_{i-1}}^{r_i}2\pi r f(r)\,dr \tag{15}$$

These results generalize Eqs. (37) and (38) in Ref. [1] to an analysis with shape functions. This analysis assumes each cylinder is transversely isotropic with the axial direction of material symmetry in the axial or z direction of the cylinders. Shear-lag analysis can therefore handle anisotropic material properties.

Next consider n concentric cylinders where cylinder i extends from r_{i-1} to r_i (see Fig. 1). The central cylinder may be solid ($r_0 = 0$) or hollow ($r_0 > 0$). Substituting $w_i''(r_i)$ from the outer edge of cylinder i and $w_{i+1}''(r_i)$ from the inner edge of cylinder $i+1$ into the imperfect interface relation (Eq. (10)) gives:

$$2\left[\frac{r_{i-1}\tau(r_{i-1},z)}{E_A^{(i)}(r_i^2-r_{i-1}^2)} - r_i\tau(r_i,z)\left(\frac{1}{E_A^{(i)}(r_i^2-r_{i-1}^2)}+\frac{1}{E_A^{(i+1)}(r_{i+1}^2-r_i^2)}\right)+\frac{r_{i+1}\tau(r_{i+1},z)}{E_A^{(i+1)}(r_{i+1}^2-r_i^2)}\right]$$
$$= \frac{r_{i-1}\tau''(r_{i-1},z)}{2G_A^{(i)}}\left\langle\left(\frac{r_{i-1}^2}{r^2}-1\right)I_i(r)\right\rangle + r_i\tau''(r_i,z)\left(\frac{\left\langle\left(\frac{r_{i-1}^2}{r^2}-1\right)O_i(r)\right\rangle}{2G_A^{(i)}}\right.$$
$$\left. - \frac{\left\langle\left(\frac{r_{i+1}^2}{r^2}-1\right)I_{i+1}(r)\right\rangle}{2G_A^{(i+1)}}\right) - \frac{r_{i+1}\tau''(r_{i+1},z)}{2G_A^{(i+1)}}\left\langle\left(\frac{r_{i+1}^2}{r^2}-1\right)O_{i+1}(r)\right\rangle - \frac{r_i\tau''(r_i,z)}{r_iD_s^{(i)}} \tag{16}$$

This result extends Eq. (45) of Ref. [1] to use shape functions and to account for imperfect interfaces. The prior analysis assumed a perfect interface, which can be recovered from this analysis by setting $D_s^{(i)} = \infty$.

For a specific problem, consider the n concentric cylinders under axial load, but zero shear stress on the inner ($r = r_0$) and the outer ($r = r_n$) surfaces (it is easy to generalize to shear loading if necessary[2]). Define a shear stress vector by

$$\vec{\tau}_r = \big(r_1\tau(r_1,z), r_2\tau(r_2,z), \cdots, r_{n-1}\tau(r_{n-1},z)\big) \tag{17}$$

Using Eq. (16) the system of equations to solve for all interfacial shear stresses is

$$[A]\frac{d^2\vec{\tau}_r}{dz^2} - [B]\vec{\tau}_r = 0 \tag{18}$$

where $[A]$ and $[B]$ are tridiagonal matrices with non-zero elements:

$$A_{i,i-1} = \frac{1}{2G_A^{(i)}}\left\langle\left(1-\frac{r_{i-1}^2}{r^2}\right)I_i(r)\right\rangle \qquad A_{i,i+1} = \frac{1}{2G_A^{(i+1)}}\left\langle\left(\frac{r_{i+1}^2}{r^2}-1\right)O_{i+1}(r)\right\rangle \tag{19}$$

$$A_{i,i} = \frac{1}{2G_A^{(i)}}\left\langle\left(1-\frac{r_{i-1}^2}{r^2}\right)O_i(r)\right\rangle + \frac{1}{2G_A^{(i+1)}}\left\langle\left(\frac{r_{i+1}^2}{r^2}-1\right)I_{i+1}(r)\right\rangle + \frac{1}{r_iD_s^{(i)}} \tag{20}$$

$$B_{i,i-1} = -\frac{2}{E_A^{(i)}(r_i^2-r_{i-1}^2)} \qquad B_{i,i+1} = -\frac{2}{E_A^{(i+1)}(r_{i+1}^2-r_i^2)} \tag{21}$$

$$B_{i,i} = \frac{2}{E_A^{(i)}(r_i^2-r_{i-1}^2)} + \frac{2}{E_A^{(i+1)}(r_{i+1}^2-r_i^2)} \tag{22}$$

The elements of the matrices depend on various averages of the shape functions. The shape functions must be specified to get numerical results, but otherwise can be left arbitrary during the shear-lag analysis process; they are part of the shear-lag parameters. Use of the shape functions in Eq. (8), which are equivalent to the assumptions in Refs. [1] and [3], gives

$$\left\langle\left(1-\frac{r_{i-1}^2}{r^2}\right)I_i(r)\right\rangle = -\frac{r_{i-1}^2}{r_i^2-r_{i-1}^2}\left(\frac{r_i^2}{r_i^2-r_{i-1}^2}\ln\frac{r_i^2}{r_{i-1}^2} - 1 - \frac{r_i^2-r_{i-1}^2}{2r_{i-1}^2}\right) \tag{23}$$

$$\left\langle\left(1-\frac{r_{i-1}^2}{r^2}\right)O_i(r)\right\rangle = \frac{r_{i-1}^2}{r_i^2-r_{i-1}^2}\left(\frac{r_{i-1}^2}{r_i^2-r_{i-1}^2}\ln\frac{r_i^2}{r_{i-1}^2} - 1 + \frac{r_i^2-r_{i-1}^2}{2r_{i-1}^2}\right) \tag{24}$$

$$\left\langle\left(\frac{r_{i+1}^2}{r^2}-1\right)I_{i+1}(r)\right\rangle = \frac{r_{i+1}^2}{r_{i+1}^2-r_i^2}\left(\frac{r_{i+1}^2}{r_{i+1}^2-r_i^2}\ln\frac{r_{i+1}^2}{r_i^2} - 1 - \frac{r_{i+1}^2-r_i^2}{2r_{i+1}^2}\right) \tag{25}$$

$$\left\langle\left(\frac{r_{i+1}^2}{r^2}-1\right)O_{i+1}(r)\right\rangle = -\frac{r_{i+1}^2}{r_{i+1}^2-r_i^2}\left(\frac{r_i^2}{r_{i+1}^2-r_i^2}\ln\frac{r_{i+1}^2}{r_i^2} - 1 + \frac{r_{i+1}^2-r_i^2}{2r_{i+1}^2}\right) \tag{26}$$

Substitution of these results and $D_s^{(i)} = \infty$ recovers all results of Refs. [1] and [3] as a special case of this new generalized shear-lag analysis for concentric cylinders.

Integration of axial equilibrium in cylindrical coordinates from r_{i-1} to r_i in cylinder i gives:[1]

$$(r_i^2 - r_{i-1}^2)\frac{d\left\langle\sigma_{zz}^{(i)}\right\rangle}{dz} = 2\big(r_{i-1}\tau(r_{i-1},z) - r_i\tau(r_i,z)\big) \tag{27}$$

It is then easy to show by induction that

$$\vec{\tau}_r = -\frac{1}{2}[I_L]\frac{d\vec{p}}{dz} \tag{28}$$

where $\vec{p}$ is a vector of axial loads in the cylinders:

$$\vec{p} = \left((r_1^2 - r_0^2)\left\langle\sigma_{zz}^{(1)}\right\rangle, (r_2^2 - r_1^2)\left\langle\sigma_{zz}^{(2)}\right\rangle, \ldots, (r_{n-1}^2 - r_{n-2}^2)\left\langle\sigma_{zz}^{(n-1)}\right\rangle\right) \tag{29}$$

and $[I_L]$ is an $(n-1)\times(n-1)$ matrix with 1 on the diagonal and in the lower half of the matrix and zero elsewhere ($[I_L]_{ij} = 1$ if $i \geq j$ or 0 if $i < j$). Substitution of Eq. (28) into Eq. (18) and integration once results in shear-lag equations for axial stresses in all the cylinders:

$$\frac{d^2\vec{p}}{dz^2} - [M_\sigma]\vec{p} = -[M_\sigma]\vec{p}_\infty \qquad \text{where} \qquad [M_\sigma] = [I_L]^{-1}[A]^{-1}[B][I_L] \tag{30}$$

and $\vec{p}_\infty$ are the far-field axial stresses (*i.e.*, axial stresses far from the ends in infinitely long cylinders where all derivatives with respect to z vanish). The elements of $[I_L]^{-1}$ are: $[I_L]^{-1}_{i,j} = 1$ if $j = i$, $[I_L]^{-1}_{i,j} = -1$ if $j = i-1$, otherwise $[I_L]^{-1}_{i,j} = 0$. As outlined in Ref. [2], Eq. (30) can be solved for all axial stresses by finding eigenvalues and eigenvectors of the matrix $[M_\sigma]$. In general, this matrix is fully populated. Finally, this analysis includes residual thermal stress by their presence is $\vec{p}_\infty$.

The above analysis defines a generalized shear-lag analysis for concentric cylinders and adds modeling of imperfect interfaces. The planar analysis for multilayered structures in Ref. [2] already uses shape functions, which makes it a generalized shear-lag analysis, but it did not include imperfect interfaces. By analogy with the cylinders analysis, where imperfect interfaces only changed the diagonal elements of the $[A]$ matrix, the planar analysis can be modified for imperfect interfaces simply by redefining $A_{i,i}$ to be

$$A_{i,i} = \frac{t_{i+1}\left\langle(1-z_{i+1})L_{i+1}(z_{i+1})\right\rangle}{G_{xy}^{(i+1)}} + \frac{t_i\left\langle z_i R_i(z_i)\right\rangle}{G_{xy}^{(i)}} + \frac{1}{D_s^{(i)}} \tag{31}$$

This result modifies Eq. (35) in Ref. [2] and thus extends planar analysis to inclusion of imperfect interfaces.

Results

Fiber/Matrix Stress Transfer

A common application for shear-lag analysis of cylinders is to study stress transfer between a fiber and a matrix. The fiber/matrix problem has two cylinders. The fiber is the central, solid cylinder. The matrix is the surrounding cylinder. The fiber and matrix volume fractions are $V_1 = r_1^2/r_2^2$ and $V_2 = (r_2^2 - r_1^2)/r_2^2$. For the fiber/matrix problem, Eq. (30) reduces to a single equation for average axial stress in the fiber:

$$\frac{d^2\left\langle\sigma_{zz}^{(1)}\right\rangle}{dz^2} - \beta^2\left\langle\sigma_{zz}^{(1)}\right\rangle = -\beta^2\left\langle\sigma_{zz,\infty}^{(1)}\right\rangle \tag{32}$$

where $\left\langle\sigma_{zz,\infty}^{(1)}\right\rangle$ is the far-field, axial fiber stress, and the shear-lag parameter, β, is

$$\beta^2 = \frac{2}{r_1^2 V_2 E_A^{(1)} E_A^{(2)}}\left(\frac{E_A^{(1)}V_1 + E_A^{(2)}V_2}{\dfrac{\langle O_1(r)\rangle}{2G_A^{(1)}} + \dfrac{1}{2G_A^{(2)}}\left\langle\left(\dfrac{r_2^2}{r^2} - 1\right)I_2(r)\right\rangle + \dfrac{1}{r_1 D_s^{(1)}}}\right) \tag{33}$$

By substituting the specific shape functions in Eq. (8) or

$$I_2(r) = \frac{r_2^2 - r^2}{r_2^2 - r_1^2} \qquad \text{and} \qquad O_1(r) = \frac{r^2}{r_1^2} \tag{34}$$

the general result becomes the specific result:

$$\beta_{opt}^2 = \frac{2}{r_1^2 E_A^{(1)} E_A^{(2)}} \left(\frac{E_A^{(1)} V_1 + E_A^{(2)} V_2}{\frac{V_2}{4G_A^{(1)}} + \frac{1}{2G_A^{(2)}} \left(\frac{1}{V_2} \ln \frac{1}{V_1} - 1 - \frac{V_2}{2} \right) + \frac{V_2}{r_1 D_s^{(1)}}} \right) \tag{35}$$

This result is identical to prior optimal results[1,3,4] when the imperfect interface parameter is $D_s^{(1)} = \infty$. The new, generalized result in Eq. (33) can now be used to evaluate prior shear-lag models and to extend fiber/matrix shear-lag methods to new capabilities.

Reinterpretation of Cox Parameter

An early shear-lag analysis by Cox[5] for fiber/matrix stress transfer used the same equation as Eq. (32) but a different shear-lag parameter:

$$\beta_{cox}^2 = \frac{4G_A^{(2)}}{r_1^2 E_A^{(1)} \ln\left(\frac{s^2}{r_1^2}\right)} \tag{36}$$

where s is the mean separation of fibers normal to their length. It was previously shown that the Cox shear-lag parameter gives very poor results for prediction of fiber/matrix stress transfer.[1] It's problems can now be studied further be examination of the shape functions, and therefore the form of the shear stresses, implied by the Cox result. The parameter s is ambiguous when using concentric cylinders. Two common assumptions are to take $s = r_2$ or $s = 2r_2$. If s is taken as equal to r_2, the Cox parameter can be seen to be a special case of the generalized shear-lag parameter when $D_s^{(1)} = \infty$ and the shape function averages are

$$\left\langle O^{(1)}(r) \right\rangle = 0 \qquad \text{and} \qquad \left\langle \left(\frac{r_2^2}{r^2} - 1 \right) I^{(2)}(r) \right\rangle = \left(1 + \frac{E_A^{(1)} V_1}{E_A^{(2)} V_2} \right) \ln \frac{1}{V_1} \tag{37}$$

Similar shape functions could be found for $s = 2r_2$, but calculations show that $s = 2r_2$ gives worse results than $s = r_2$ judged by comparison to numerical results.[1] The results here assumed $s = r_2$.

There are an infinite number of shape functions with the above averages. To get a specific result, the shape functions were assumed to be cubic in the fiber and quadratic in the matrix. Using boundary conditions for shape functions, two possible Cox shape functions are

$$O^{(1)}(r) = \frac{r^2}{r_1^2} \left(1 + c_1 \frac{r_1 - r}{r_1} \right) \qquad \text{and} \qquad I^{(2)}(r) = \frac{r_2 - r}{r_2 - r_1} + c_2 \frac{(r_2 - r)(r_1 - r)}{r_2^2 - r_1^2} \tag{38}$$

where c_1 and c_2 are dimensionless constants. A cubic form in the fiber was needed to simultaneously satisfy zero average shape function and zero shear stress at $r = 0$. Substituting these forms into the Cox averages (Eqs. (15) and (37)) and solving for c_1 and c_2 gives

$$c_1 = -5 \tag{39}$$

$$c_2 = \frac{\frac{7+\sqrt{V_1}-2V_1}{3} + \left(\frac{E_A^{(1)} V_1 + E_A^{(2)} V_2}{E_A^{(2)}} - \frac{1}{1-\sqrt{V_1}} \right) \log(\frac{1}{V_1})}{\frac{V_1 - 2\sqrt{V_1} - 5}{6} + \frac{\sqrt{V_1}}{V_2} \log(\frac{1}{V_1})} \tag{40}$$

Figure 3 has sample plots for the radial dependence of the shear stress for $r_2/r_1 = 3$ ($V_1 = 11\%$) with $E_A^{(1)}/E_A^{(2)} = 10$. The shear stress was normalized to the interfacial shear stress. The optimal shear stress

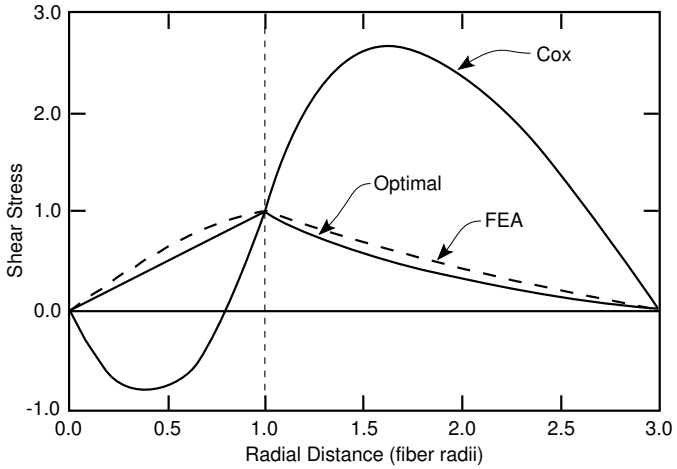

Fig. 3. A comparison of the radial dependence of the shear stress as assumed in an "optimal" shear-lag analysis, as "implied" by the Cox shear-lag parameter, and as calculated by finite element analysis ("FEA"). All results were normalized to the interfacial shear stress.

used the shape functions in Eq. (34). The optimal assumption has shear stress that is zero at the center and increases linearly to the fiber/matrix interface. The shear stress then decays to reach zero on the matrix surface. The shape functions consistent with the Cox parameter are unreasonable. The shear stress at the center was set to zero, but then must oscillate around zero to maintain shape function average equal to zero (see Eq. (37)). In the matrix the shear stress has an unlikely shape required to satisfy the unrealistically high shape function average (see Eq. (37)).

To confirm problems with Cox shear stress assumptions and acceptability of the optimal shear stress assumptions, the form of the shear-lag shear stresses were compared to finite element calculations. In finite element analysis, the radial dependence of the shear stress (after normalization to the interfacial shear stress) varies somewhat as a function of distance from the fiber break. The most important shear stress effects are near the fiber break. Therefore, the average shear stress near the break, at a distance of one fiber diameter ± one fiber radius, was calculated as a function of radial position. The finite element (FEA) shear stresses shown in Fig. 3 are close to the optimal shear stresses and are very different than the Cox shear stresses.

Correction of Low Fiber Volume Fraction Analysis

A problem with all prior shear-lag analyses of fiber/matrix stress transfer is that they break down at low fiber volume fraction. This problem can be fixed using shape functions. The shear-lag solution for stress transfer from an isolated fiber break is

$$\frac{\left\langle \sigma_{zz}^{(1)} \right\rangle}{\left\langle \sigma_{zz,\infty}^{(1)} \right\rangle} = 1 - e^{-\beta z} \tag{41}$$

where z is the distance from the fiber break. The fiber stress is zero at the break ($z = 0$) and asymptotically approaches the far-field stress by the exponential function. The shear-lag parameter characterizes the rate of stress stress transfer. For example, the distance required for the stress to reach half the far-field stress is

$$z_{50} = \frac{\ln 2}{\beta} \tag{42}$$

The problem with prior shear-lag parameters is that they approach zero as fiber volume fracture gets small or

$$\lim_{V_1 \to 0} \beta_{cox} = \lim_{V_1 \to 0} \beta_{opt} = 0 \tag{43}$$

with the result being that $\lim_{V_1 \to 0} z_{50} = \infty$. This bad limit is caused by the $\ln(1/V_1)$ terms, which arises from the matrix $I^{(2)}(r)$ shape function average, in the denominators that approaches ∞ as the fiber volume fraction approaches zero. In a generalized shear-lag analysis, the zero limit problem can be fixed by changing the shape function such that the average adds a small constant χ to the log term. A potential, corrected shear-lag parameter is then

$$\beta_{cor}^2 = \frac{2}{r_1^2 E_A^{(1)} E_A^{(2)}} \left(\frac{E_A^{(1)} V_1 + E_A^{(2)} V_2}{\frac{V_2}{4G_A^{(1)}} + \frac{1}{2G_A^{(2)}} \left(\frac{1}{V_2} \ln \frac{1}{V_1 + \chi} - 1 - \frac{V_2}{2} \right) + \frac{V_2}{r_1 D_s^{(1)}}} \right) \tag{44}$$

This new parameter has a well defined limit at zero fiber volume fraction of

$$\lim_{V_1 \to 0} \beta_{cor}^2 = \frac{4G_A^{(2)}}{r_1^2 E_A^{(1)} \left(\frac{G_A^{(2)}}{2G_A^{(1)}} - \ln \chi - \frac{3}{2} + \frac{2G_A^{(2)}}{r_1 D_s^{(1)}} \right)} \tag{45}$$

This limit allows predictions of fiber/matrix stress transfer for a fiber in an infinite amount of matrix and includes effects of fiber anisotropy and an imperfect interface.

The question remains — is there a constant χ that gives good results for all combinations of fiber and matrix properties? To search for χ, predictions of z_{50} using β_{cor} were compared to finite element results. Although finite element analysis can not model a fiber in an infinite matrix either, it can vary fiber volume fraction and the results for z_{50} can be observed to approach a limit at low fiber volume fraction. The zero-volume-fraction limit was found by extrapolation. The procedure was as follows:

1. Given a matrix modulus, $E_A^{(2)}$, the fiber was assumed to have modulus $RE_A^{(2)}$ (*i.e.*, the fiber/matrix modulus ratio was R). The fiber and matrix were first assumed to be isotropic with $\nu_A^{(1)} = 0.25$ and $\nu_A^{(2)} = 0.33$. The shear moduli were thus $G_A^{(1)} = RE_A^{(2)}/(2(1+\nu^{(1)}))$ and $G_A^{(2)} = E_A^{(2)}/(2(1+\nu^{(2)}))$

2. Two concentric cylinders were meshed in an axisymmetric analysis using 8-noded isoparametric elements. Two separate meshes were created for $V_1 = 2\%$ and for $V_1 = 1\%$. These geometries corresponded to $r_2/r_1 = 7.07$ and $r_2/r_1 = 10$, respectively.

3. Finite element analysis was run[11] as a function of R and the average stress in the fiber was calculated along the axis of the fiber. The finite element convergence was verified by varying the number of elements until the stress transfer results converged.

4. The point where stress reached half the far-field stress was located for $V_1 = 2\%$ and for $V_1 = 1\%$. These results were extrapolated to zero fiber volume fracture to get numerical results for z_{50} for a fiber in an infinite amount of matrix.

5. Finite element analysis also required finite fiber length. The numerical z_{50} results were for an analysis that extended 25 fiber diameters from the break. This length was verified to be sufficient for analysis of an isolated break by analytical calculations[1,9] and by comparison to results with shorter analysis lengths that showed only negligible effects of fiber length for lengths greater than 15 fiber diameters.

6. To see how shear-lag analysis can handle anisotropic fibers, the finite element analyses were repeated for anisotropic fibers. The matrix and fiber moduli were again assumed to be $E_A^{(2)}$ and $RE_A^{(2)}$, respectively. The matrix was assumed to be isotropic with $\nu_A^{(2)} = 0.33$ and $G_A^{(2)} = E_A^{(2)}/(2(1+\nu^{(2)}))$. In analogy with typical carbon fibers properties, the remaining transversely isotropic fiber properties were assumed to be $G_A^{(1)} = RE_A^{(2)}/10$, $E_T^{(1)} = RE_A^{(2)}/15$, $\nu_A^{(1)} = 0.20$, and $\nu_T^{(1)} = 0.25$.

Figure 4 compares shear-lag prediction of z_{50} to finite element results for both isotropic and anisotropic fibers. The symbols are finite element results. The curves are shear-lag predictions that were fit by varying χ. The fits used $\chi = 0.009$. which appears to be a universal constant that gives good results for stress transfer

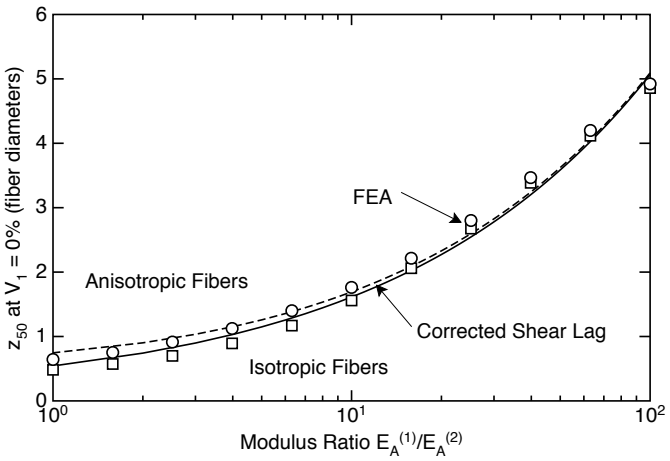

Fig. 4. Comparison of z_{50} for a fiber in an infinite amount of matrix calculated by shear-lag analysis (curves) and by finite element analysis (symbols). The shear-lag analysis used the corrected parameter, β_{cor}, with $\chi = 0.009$. The two sets of results are for isotropic (solid curve and squares) or anisotropic fibers (dashed curve and circles).

at low fiber volume fraction for any fiber/matrix modulus ratio and for both isotropic and anisotropic fibers. The effect of fiber anisotropy is always small, but is slightly larger when the modulus ratio is less then 10. Shear-lag predictions with β_{cor} are consistent with all effects of anisotropy. In contrast, the Cox parameter depends only on fiber axial modulus and not on fiber shear modulus. That parameter can not account for any effects of fiber anisotropy.

The final question was whether the corrected shear-lag parameter with $\chi = 0.009$ also gives a smooth transition to β_{opt}, which is known to work well at higher volume fractions.[1] Figure 5 plots z_{50} as a function of fiber volume fraction for three different modulus ratios all with isotropic fibers. The predictions using the corrected results (solid curves) converge rapidly to the optimal results (dotted curves) at higher volume fractions. At low fiber value fractions, the corrected results converge to numerical results (see Fig. 4) while the optimal results break done and approach infinity. In other words, the corrected shear-lag parameter gives good predictions of fiber/matrix stress transfer for any fiber volume fraction and for any fiber/matrix modulus ratio. Certainly the modification to the average of $I^{(2)}(r)$ to add χ to the log term in the denominator is not the only possible solution to the low fiber volume fraction problem. The shape function averages could be modified in other ways such as rescaling of volume fraction to effective volume fractions that never approach zero. The method chosen here is a minimal change to prior shear-lag parameters, provides a smooth transition between low and high fiber volume fraction results, and has been confirmed by a battery of numerical calibrations to work for any combination of fiber and matrix properties that are likely to be encountered in stress transfer problems.

Imperfect Interface Example

The development of analytical models for stress transfer require both verification and validation.[12] In verification, one seeks to confirm that the approximate methods used in the modeling have solved the assumed mechanics problem with sufficient accuracy. The above sections and the results in Ref. [1] show that shear-lag analysis of two cylinders is a verified method for calculations of fiber/matrix stress transfer. Verification is best done by comparison to numerical solution of the same mechanics problem. In validation, one compares analytical models to experimental results to demonstrate use of those models for interpretation and analysis of real composites. If there are discrepancies between experiments and verified models, those discrepancies can not be due to the analysis methods; they can only be due to weaknesses in the underlying physical model. For example, if shear-lag predictions for stress transfer at a perfect interface do not agree with experiments, the disagreements are not due to the shear-lag methods but must be due either to the assumption of a perfect interface or to the assumption of linear elastic material properties. Here some experimental results on stress

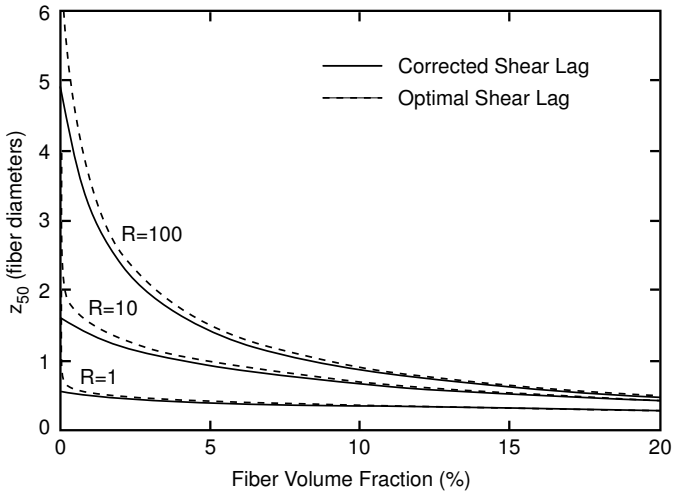

Fig. 5. Comparison of z_{50} as a function of fiber volume fracture calculated using β_{cor} with $\chi = 0.009$ (solid curves) or using β_{opt} (dashed curves). The three curves are for three different fiber/matrix modulus ratios (R).

transfer between carbon fibers and an epoxy matrix[13] were interpreted. Because the experiments are at low strain ($< 0.4\%$ strain), where these materials are likely to be linear elastic, all discrepancies were assumed to be caused by an assumption of a perfect interface. By varying the interface parameter, D_s, it was possible to fit shear-lag predictions to experimental results and therefore to quantify the quality of the interface.

Reference [13] describes a set of experiments on a high modulus (HM) carbon fiber embedded in a room temperature cured epoxy. The fibers were embedded in the matrix and the stress in the fiber as a function of distance from the fiber end was measured using Raman spectroscopy at several levels of applied strain. Details about the experimental procedures are given in Ref. [13]. Figure 6 compares shear-lag predictions (solid curves) to experimental results (symbols). Because a small fiber was embedded in a large amount of matrix, the shear-lag analysis assumed $V_1 = 0$ and used the low-fiber-volume-fraction result above with the universal $\chi = 0.009$ (see Eq. (44)). The fiber and matrix properties are listed in the caption of Fig. 6. The shear-lag predictions with a perfect interface, or with $D_s = \infty$, predict stress transfer faster than observed in experiments. By varying D_s, the experimental results could be fit to shear-lag predictions. The best fit gives an experimental determination of the interface parameter to be $r_1 D_s = 300$ MPa.

Also plotted in Fig. 6 are stress transfer predictions done using a much more sophisticated stress transfer analysis based on expansion of stresses using a Bessel-Fourier series.[9] The Bessel-Fourier analysis is a full axisymmetric analysis of fiber/matrix stress transfer that includes imperfect interface effects and is nearly exact. The only approximation is that the axial stress at the fiber break is zero in an average sense but not zero at each location on the break surface. The shear-lag analysis (solid curves) and the Bessel-Fourier analysis (dashed curves) agree well for both a perfect and an imperfect interface. This agreement is further verification of the shear-lag method. The Bessel-Fourier analysis is much more complex and requires evaluation of 50 or more terms for convergence. The results here show that shear-lag analysis provides an acceptable alternative for stress transfer calculations in a far simpler method. Both shear-lag analysis and Bessel-Fourier analysis lead to the same interface parameter when interpreting experiments. A complete imperfect interface in an axisymmetric analysis may have displacement discontinuities in both the axial and normal directions. The Bessel-Fourier analysis includes transverse displacements and therefore can model both types of discontinuities. Shear-lag analysis can only model axial displacement discontinuities. Because of the nature of the interfacial shear stresses and the predominantly compressive interfacial radial stresses, the axial discontinuity is the more import interface effect for stress transfer problems under axial load.[9,10]

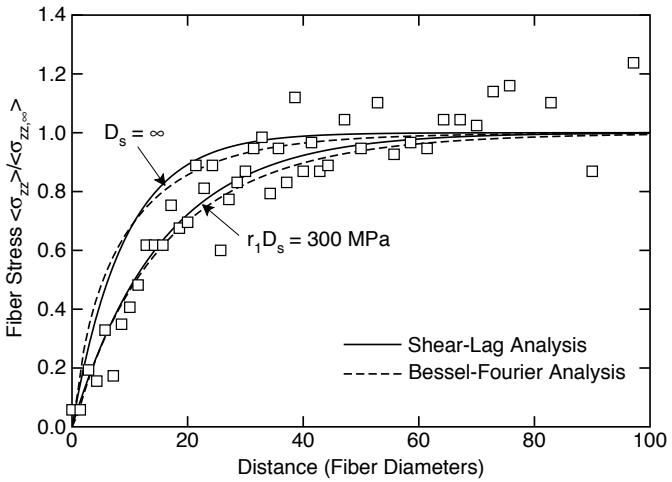

Fig. 6. Comparison of both shear-lag analysis and Bessel-Fourier analysis to experimental results (symbols) of stress transfer into an HM carbon fiber at an applied strain 0.4%. The mechanical properties of the fiber and matrix were $E_A^{(1)} = 390$ GPa, $G_A^{(1)} = 20$ GPa, $E_A^{(2)} = 2.6$ GPa, and $G_A^{(2)} = 0.97$ GPa.

Conclusions

Prior optimal shear-lag methods with perfect interfaces[1,2] were extended to generalized shear-lag methods and to account for imperfect interfaces. A generalized shear-lag analysis uses shape functions to describe the transverse variation in shear stress in each cylinder or layer. The shear-lag equation and solution can be expressed in terms of averages of arbitrary shape functions. An optimal shear-lag analysis uses default shape functions for cylindrical or planar problems. By deviating from default shape function for certain problems, however, the accuracy and applicability of shear-lag analysis can be extended. Here shape functions were used to further investigate inaccuracies with the Cox shear-lag parameter and to extend fiber/matrix shear-lag analysis to handle low fiber volume fractions. The low-fiber-volume-fraction shape function and imperfect interface effects were used to interpret Raman experiments for stress transfer.

Acknowledgements

The ideas for this paper came from my presentation to a Marie Curie training Event at the 11$^{\text{th}}$ European Conference on Composite Materials (Contract number: MLCF-CT2003-504-333). I thank Prof. Costas Galiotis for inviting me to prepare the training event and the participants in that event for questions that seeded the results in this paper.

References

1. Nairn, J. A., "On the Use of Shear-Lag Methods for Analysis of Stress Transfer in Unidirectional Composites," *Mechanics of Materials*, **26** (1997), 63–80.
2. Nairn, J. A. and Mendels, D.-A., "On the Use of Planar Shear-Lag Methods for Stress-Transfer Analysis of Multilayered Composites," *Mechanics of Materials*, **33** (2001), 335–362.
3. McCartney, L. N., "Analytical Models of Stress Transfer in Unidirectional Composites and Cross-Ply Laminates, and Their Application to the Prediction of Matrix/Transverse Cracking," *Local Mechanics Concepts for Composite Material Systems*, eds., J. N. Reddy and K. L Reifsnider, Proc. IUTAM Symposium, Blacksburg, VA, (1992), 251–282.
4. Nayfeh, A. H., "Thermomechanically Induced Interfacial Stresses in Fibrous Composites," *Fibre Sci. & Tech.*, **10** (1977), 195–209.

5. Cox, H. L., "The Elasticity and Strength of Paper and Other Fibrous Materials," *Brit. J. Appl. Phys.*, **3** (1952), 72–79.
6. Mendels, D.-A., Page, S. A., Månson, J.-A. E., and Nairn, J. A., "A Compression-Loaded Double Lap Shear Test: Part 1, Theory," *Int. J. Adhes. & Adhes.*, **in press** (2002).
7. Hashin, Z., "Thermoelastic Properties of Fiber Composites With Imperfect Interface," *Mech. of Materials*, **8** (1990), 333–348.
8. Nairn, J. A., Liu, Y. C., and Galiotis, C., "Analysis of Stress Transfer from the Matrix to the Fiber Through an Imperfect Interface: Application to Raman Data and the Single-Fiber Fragmentation Test," *ASTM*, **STP 1290** (1995), 47–65.
9. Nairn, J. A. and Liu, Y. C., "Stress Transfer into a Fragmented, Anisotropic Fiber Through an Imperfect Interface," *Int. J. Solids Structures*, **34** (1997), 1255–1281.
10. Paipetis, A., Liu, Y. C., Galiotis, C., and Nairn, J. A., "Stress Transfer from the Matrix to the Fiber in a Fragmentation Test: Raman Experiments and Analytical Modeling," *J. Comp. Mat.*, **33** (1999), 377–399.
11. Nairn, J. A., "JANFEA, Finite Element and Material Point Method Software for the Macintosh," `http://www.eng.utah.edu/ nairn/JANFEA/`.
12. Oberkampf, W. L. and T. G. Trucano, "Verification and Validation in Computational Fluid Dynamics," *Sandia Report SAND2002-0529* (2003).
13. Melanitis, N., Galiotis, C., Tetlow, P. L., and Davies, C. K. L., "Interfacial Shear Stress Distribution in Model Composites Part 2: Fragmentation Studies on Carbon Fibre/Epoxy Systems," *J. Comp. Mat.*, **26** (1992), 574–610.